

# IMPACT OF UNDULATOR WAKEFIELDS AND TAPERING ON EUROPEAN X-RAY FEL PERFORMANCE\*

I. Zagorodnov<sup>#</sup>, M. Dohlus, T. Limberg, DESY, Hamburg, Germany

## Abstract

The European x-ray Free-Electron Laser (XFEL) requires an electron beam with a few kA peak current. The interaction between the high-current electron bunch and the undulator vacuum chamber affects the FEL performance. To study the expected performance in the presence of the calculated wakefields we are doing start-to-end simulations.

## INTRODUCTION

The European XFEL is based on self-amplified spontaneous emission (SASE) and requires an electron beam with a few kA peak current and a small-gap undulator system of up to 260 m in length [1]. The electromagnetic interaction between the high-current electron bunch and the undulator vacuum chamber affects the FEL performance. In this paper we estimate the induced wakefields in an elliptical pipe geometry taking into account main geometrical variations of the chamber. To study the expected performance in the presence of the calculated wakefields we are doing start-to-end simulations with the codes ASTRA [2], CSRtrack [3] and Genesis [4]. In order to compensate the impact of wake fields on the FEL performance, an adiabatic change of undulator parameters is applied.

## START-TO-UNDULATOR SIMULATION

The beam dynamics in the rf photo injector and the linac has been modeled with the codes ASTRA and CSRtrack. The particles are tracked taking into account space charge effects with the code ASTRA to the 130 MeV point. For all other linac sections, transport matrices and a semi-analytic model for longitudinal space charge effects are used to propagate particle phase space.

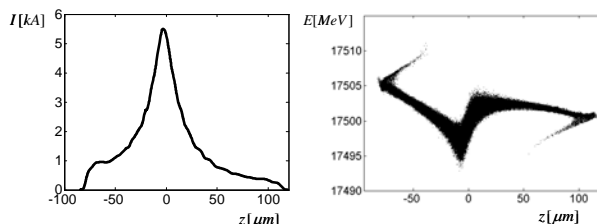


Figure 1: Current profile and longitudinal phase space at the undulator entrance (1nC at 17.5GeV)

The wake field effects of the TESLA cryomodules and other elements are calculated with code ECHO [5] and are included in the simulations.

The beam dynamic in CSRtrack uses the one dimensional approach. The simulation starts with a 1nC

bunch with a peak current of about 50A from the photo cathode. The bunch is compressed in two stages at 500MeV by a factor of 20 and at 2 GeV by a factor of 5. The calculated current profile and the longitudinal phase space are shown in Fig.1.

The results of this previous start-to-end simulation have been checked with a more thorough approach, where all linac sections up to 3 GeV have been calculated with ASTRA and the compressor chicanes with a 3D method in CSRtrack. The differences in the final particle distribution were not big enough to have an impact on the results of this paper.

## Wakefields in the Undulator

The effect of undulator wakefields becomes noticeable as gain reduction when the variation in energy becomes big compared to the FEL bandwidth, i.e.  $\Delta E_{wake} / E \geq \rho$ . In the case of SASE2 parameters [1] this gives the condition  $W_z > 41 \text{ kV}/(\text{nC} \times \text{m})$  on the amplitude of wake potential per length.

There are three major sources of wakefields within the undulator: resistive walls, rough surfaces and geometric discontinuities. Resistive and surface roughness wakefields for beam pipes with smooth shallow corrugations have been calculated in [6]. It is found that the roughness of the investigated surface contributes similarly to the wake as an oxide layer ( $\epsilon_r \approx 2$ ) with 2% of the rms thickness of that roughness. An estimated rms thickness below 250 nm increases the surface effects by approximately 10% and is therefore neglected. The calculation of the geometrical and resistive wakefields is described in the following sections.

## The Resistive-Wall Wakefield

To estimate the resistive wall wakefields we use the results of [7]. For a round pipe of radius  $a$  the longitudinal impedance is given by

$$Z(k) = \frac{2}{ca} \left[ \frac{\lambda}{k} - \frac{ika}{2} \right]^{-1}, \quad \lambda = \sqrt{\frac{2\pi|k|}{c}} [i + \text{sign}(k)], \quad (1)$$

where  $k = \omega/c$  and ac conductivity  $\tilde{\sigma}$  is given by

$$\tilde{\sigma} = \sigma (1 - ikc\tau)^{-1}.$$

We take the half-height of the elliptical pipe  $a = 3.8 \text{ mm}$  (see Fig. 2) as the radius of the round pipe and consider it as a conservative estimation of the wakefields for the elliptical pipe.

## The Effect of Geometrical Elements

The beam tube inside of the undulator has elliptical cross section with a thin pumping slot along the whole undulator segment as shown in Fig. 2.

\*Work supported in part by EUROFEL project

<sup>#</sup>igor.zagorodnov@desy.de

The results [10] based on Bethe's theory are not applicable for this case since the width of the slot  $w = 1\text{mm}$  is much bigger than the RMS length  $\sigma = 25\mu\text{m}$  of the Gaussian bunch used in the following calculations.

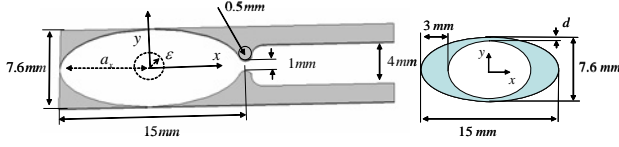


Figure 2: The undulator pipe and the absorber geometry.

At the same time it is difficult to estimate the effect of the slot numerically as the effect is presumably small and numerical errors could spoil the results. In order to obtain a convincing estimation we have built a parametric model of the long slot and fitted the parameters of the model numerically [9]. The time-domain simulations with electrodynamic code ECHO [5] have been used for this purpose. The calculations shown in [9] results in the parametric model

$$k_{loss}^{out} = O(\theta^{1.8} \sigma^{-1} \ln(h/a)), \quad k_{loss}^{in} = O(\theta/a), \quad (2)$$

where  $\theta$ ,  $a$ ,  $h$  are geometric parameters defined in [9] and  $\sigma$  is the bunch length. From this model we obtain the estimation  $k_{loss} \approx 0.2 \text{ V/pC}$ .

Table 1: Wake parameters

	Loss, V/pC	Spread, V/pC	Peak, V/pC
absorber	42	16	-58
pumping slot (Fig.2)	<0.2	<0.1	>-0.3
pump	9	4	-13
bellow	13	5	-18
flange gap	6	2.4	-8.5
<b>total geom.</b>	<b>70</b>	<b>25</b>	<b>-95</b>

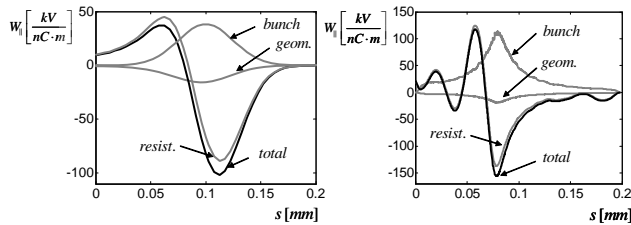


Figure 3: Wakes for Gaussian and simulated current profiles.

In order to protect the undulator from synchrotron radiation, absorbers should be installed in each undulator section. The absorber has the cross-section shown in Fig.2 and its length is 10 mm. We have considered two variants of absorber:  $d = 0.5\text{mm}$  and  $d = 0$ . From direct time-domain calculations [5] the estimations for the loss and the kick factors are (in V/pC):  $k_{loss} = 84$ ,  $k_{kick,x} = 436x/\text{m}$ ,  $k_{kick,y} = 301y/\text{m}$  for  $d = 0.5\text{mm}$  and

$$k_{loss} = 42, \quad k_{kick,x} = 486x/\text{m}, \quad k_{kick,y} = -130y/\text{m} \text{ for } d = 0.$$

The calculated wake parameters for a Gaussian bunch with RMS length of  $\sigma = 25\mu\text{m}$  are gathered in Table 1.

### Wakepotential for the Simulated Current Profile

The results calculated in the previous sections for copper pipe and Gaussian bunch with RMS length  $\sigma = 25\mu\text{m}$  are shown in Fig. 3.

We see that the geometrical wake is resistive in the nature and since it can be written as

$$W_{||}(s) = cZ_{hi}\lambda(s), \quad (3)$$

where  $\lambda$  is the longitudinal bunch profile. From the fit of the above expression to the numerical results we have found that  $Z_{hi} = 3.36[\Omega]$ . Using Eq. 3 for the geometric wake and Eq. 1 for the resistive wall wake we have obtained the wake potentials for the simulated current profile (see Fig. 1). The wakes are shown in Fig. 3. The resistive wall wake is dominant and its amplitude depends strongly on the bunch shape.

## UNDULATOR-TO-END SIMULATION

We have followed the standard way [10] of preparing input data for an FEL code: a macro-particle distribution at the undulator entrance was cut into longitudinal slices. A mean energy, rms energy spread, current, rms emittance were calculated for each slice. Then each slice was perfectly matched to the undulator entrance and all centroids were placed on the ideal orbit.

Table 2: The SASE2 parameters

Parameter	Symbol	Unit	Value
radiation wavelength	$\lambda$	nm	0.1
energy	$E$	GeV	17.5
energy spread	$\sigma_E$	MeV	1
undulator parameter	$K_{rms}$		1.97
emittance	$\epsilon_n$	mm*mrad	0.7
peak current	$I$	kA	5
average beta function	$\beta$	m	17.25
undulator section length	$L_{sect}$	m	5
intersection length	$L_{inters}$	m	1.1
total length	$L_{total}$	m	260
undulator period	$\lambda_u$	m	0.048

In this section we evaluate with the help of code Genesis [4] the effect of wakefields on the XFEL performance for radiation of a wavelength of 0.1 nm.

A reliable method to increase the FEL undulator efficiency and compensate energy losses in the bunch consists in an adiabatic change of undulator parameters [11, 12]. For a variable gap device, such as the TESLA FEL undulators we can write

$$\frac{\Delta K_{rms}}{K_{rms}} \approx -\frac{\Delta g}{g} \left( -5.068 \frac{g}{\lambda_u} + 3.04 \left( \frac{g}{\lambda_u} \right)^2 \right),$$

where  $K_{rms} = 93.4 \lambda_u B_u / \sqrt{2}$ . For the set of parameters given in Table 2 we obtain a law for the gap change

$$\Delta g = -0.0124 \Delta K_{rms} / K_{rms}$$

and the efficiency parameter  $\rho$  [11] is equal to  $7.1 \cdot 10^{-4}$ .

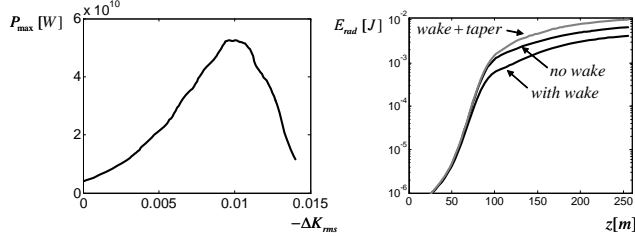


Figure 4: The maximum power dependence on tapering (left) and the radiation power along the undulator (right).

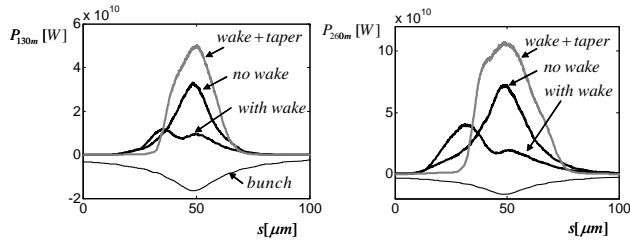


Figure 5: The radiation power in the middle (left) and at the end of the undulator (right).

In order to find optimal taper for the calculated earlier wake potential we used the amplifier steady-state model with effective power of the shot noise [11]

$$W_{sh} = 3\rho W_b \left( N_c \sqrt{\pi \ln N_c} \right)^{-1} = 11800 [\text{W}]$$

and energy loss  $W_{||} = 150 \text{ kV/nC/m}$ . The dependence of maximal power on change of the undulator parameter is shown in Fig. 4. The optimal taper is about

$$\Delta g = -0.0124 \Delta K_{rms} / K_{rms} = 60 \cdot 10^{-6} [\text{m}]$$

Next we have done numerical simulations of SASE FEL with wake potential shown in Fig. 3. The calculated results are presented in Fig. 5. As one can see from this figure, in the absence of wakefields the radiation pulse energy is 2.3 mJ at 130m. It is reduced to 1.2 mJ by undulator wakefields. The optimal linear undulator tapering  $\Delta K/K \approx 7\rho$  allows to avoid the degradation and to increase the radiation energy up to 3.5 mJ at 130 m.

Realization of the linear taper demands the undulator gap variation of only  $60 \mu\text{m}$  per 260 m that imposes severe tolerance requirements on the undulator alignment.

The undulator consists of 42 sections. In order to estimate tolerance requirements on undulator gap we have done series of steady state and SASE simulations where the optimal taper was disturbed by undulator gap error  $\delta g$  in each section. The gap error  $\delta g$  was distributed in accordance with Gaussian law. The maximum of

radiation energy was found along first 130 meter of undulator. The normalized maximal mean power  $\langle E_{max}^{\delta g} \rangle$  vs. gap error  $\delta g$  is shown in Fig. 6 on the left. On the right the fluctuations of the radiation energy  $\sigma_E$  for  $\delta g = 5 \mu\text{m}$  are plotted. For this gap error we expect the decrease of the expected radiation energy by 10% with RMS energy deviation of 16%.

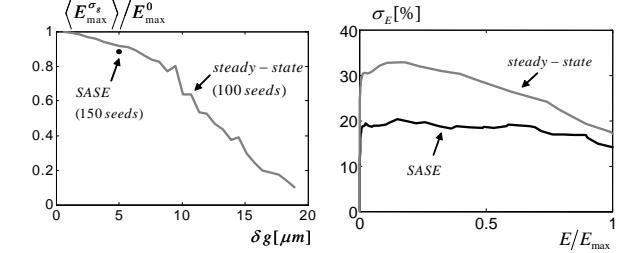


Figure 6: The radiation energy vs. the gap error and the energy fluctuations for  $\delta g = 5 \mu\text{m}$ .

## CONCLUSION

In this report we present calculations of the bunch shape at the undulator entrance in the European XFEL and the resulting wake fields in the undulator vacuum chamber. The shape of the bunch is smooth and quite close to the design parameters [1]. The wakes induced by the bunch in the undulator vacuum chamber are dominated by the resistive wall wake and reduce the radiation pulse energy by 50% in the case of an untapered undulator. Tapering the gap height linearly with a difference of  $60 \mu\text{m}$  in the case of the 260 m long SASE undulator recovers and increases the radiated power. The taper compensates effectively the energy losses due to the wakefields and the FEL process, but presence of wakefields demands deeper tapering.

We would like to thank V. Balandin, R. Brinkmann, S. Reiche, E. Saldin, E. Schneidmiller and M. Yurkov for useful discussions.

## REFERENCES

- [1] TESLA Technical Design Report, DESY 2001-011.
- [2] K. Flöttmann, ASTRA User manual.
- [3] M. Dohlus, TESLA-FEL-2003-05, DESY, 2003.
- [4] S. Reiche, NIM Phys. Res. A 429 (1999).
- [5] I. Zagorodnov, T. Weiland, Phys Rev STAB 8 (2005).
- [6] M. Dohlus, TESLA 2001-26, 2001.
- [7] K.L.F. Bane, G.V. Stupakov, SLAC-PUB-10707, 2004.
- [8] G.V. Stupakov, Phys.Rev. E 51 (1995).
- [9] M. Dohlus et al., TESLA-FEL 2005-10, 2005.
- [10] M. Dohlus et al, NIM Phys. Res. A 530 (2004).
- [11] E.L. Saldin, E.A. Schneidmiller, M.V. Yurkov, The Physics of Free Electron Lasers (Springer, Berlin, 1999).
- [12] S. Reiche, H. Schlarb, NIM Phys. Res..A 445 (2000).